Behavioural modification of local hydrodynamics by asteroids enhances reproductive success

Barrie Dams[a] OrcID: 0000-0001-7081-5457

Chris E. Blenkinsopp[a*] OrcID: 0000-0001-5784-2805

Daniel O. B. Jones[b] OrcID: 0000-0001-5218-1649

[a] Water, Environment and Infrastructure Resilience Research Unit, Department of Architecture and Civil Engineering, University of Bath, Bath BA2 7AY, UK

[b] National Oceanography Centre, University of Southampton Waterfront Campus, European Way, Southampton, SO14 3ZH, UK

* corresponding author:

c.blenkinsopp@bath.ac.uk

+44 (0)1225 386715

Water, Environment and Infrastructure Resilience Research Unit

Department of Architecture and Civil Engineering

University of Bath

Bath

BA2 7AY

UK

ABSTRACT

The reproduction of apex species, such as sea stars, is important for sustaining many marine ecosystems. Many sea star species reproduce externally, introducing gametes in the turbulent benthic boundary layer. Sea stars often aggregate and adopt characteristic behaviour, such as arched posturing, while spawning. Here we quantify, for the first time, the hydrodynamic advantages of postural changes and the extent to which they enhance the efficiency of external reproduction. Hydrodynamic and fertilisation kinetic theoretical modelling were used to provide context and comparison. The arched posture was clearly important in the downstream advection of gametes. Digital particle image velocimetry, acoustic doppler velocimetry and dye release experiments indicated reduced wake and lower shear stresses downstream of arched sea stars, which increased downstream transport of gametes compared to those in the flat position. In all cases, sperm concentration decay rates of two orders-of-magnitude over distances less than 20 cm were inferred from fluorometry, confirming the requirement for close aggregation. The level of turbulence and hence downstream gamete dilution was increased by greater current speeds and a rougher seabed. Both an arched posture and hydrodynamic conditions may improve external reproduction efficiency, with behavioural mechanisms providing the primary contribution.

Key words: Sea star; arching; spawning; turbulence; sperm concentration; flow velocity.

1. INTRODUCTION

Sea stars are an important group (Lawrence, 2013), playing a crucial ecological role by serving as voracious predators, prey and detritivores, as well as regulating and maintaining ecosystem structure and functioning (Clark, 1968; Paine, 1969; Uthicke et al., 2009). The majority of sea star species are dioecious and spawn externally (Naylor, 2011). For most species, males and females congregate on an annual basis and release gametes into the turbulent benthic boundary layer (Barker and Nichols, 1983). Sea water temperature change is considered a factor in triggering the external spawning of gametes (Hancock, 1958; Minchin, 1987; Mercier and Hamel, 2009). During spawning events, asteroids congregate in large numbers (Hancock, 1958; Clark, 1968) and females release millions of eggs into the water column (*Asterias* sp. may release 2.5 million eggs per individual over two hours; Clark, 1968), with males ejecting spermatozoa to facilitate external fertilisation (Clark, 1968). Many echinoderms modify their behaviour during spawning, for example by aggregating (Young et al., 1992) or modifying their position and posture, for example by rising from a flat to an arching posture (Fig. 1). The benefits gained by these behaviours have not been quantified.

Asterias rubens Linnaeus, 1758, is one of the most common sea stars in the North Atlantic and often used as a model species to represent the Asteroidea, owing to its typical size, morphology and function (Vevers, 1949; Barker and Nichols, 1983; Nichols and Barker, 1984). *A. rubens* inhabits both smooth sandy surfaces as well as rough rocky surfaces (Naylor, 2011). The size of sexually mature specimens is between 10 and 30 cm diameter (Hayward and Ryland, 1995). Spawning occurs during spring months when gonads are fully ripe (Nichols and Barker, 1984).

External fertilisation in the turbulent benthic boundary layer would appear to be an inefficient method of reproduction (Denny and Shibata, 1989), but is commonly used by a range of invertebrates and vertebrates (Yund, 2000; Crimaldi and Zimmer, 2014). The motility and locomotory abilities of released gametes is negligible (Denny, 1988) and viability of oocytes (<24 h) and spermatozoa (<5 h) is short (Vogel et al., 1982; Denny and Shibata, 1989; Williams and Bentley, 2002). Therefore, successful external fertilisation is reliant on high gamete concentrations and turbulent mixing (Levitan et al., 1991; Crimaldi and Zimmer, 2014). Flow velocities of less than 0.10 m/s on an uneven substrate can provide sufficient turbulent mixing to aid successful fertilisation (Denny, 1988). Inadequate turbulence may result in released gametes from each sex failing to meet before they become ineffective (Yund, 2000) and excessive turbulence results in gametes being rapidly diluted, reducing levels of fertilisation success (Pennington, 1985; Denny and Shibata, 1989). At a distance of more than 1.00 m, gametes are expected to become too diluted for successful fertilisation to occur (Pennington, 1985; Denny and Shibata, 1989). Optimal downstream sperm concentrations vary across taxa, for example, 10^5 sperm ml^{-1} for gastropods, with no fertilisation occurring below 10^2 sperm ml^{-1} (Baker and Tyler, 2001), and 10^2 - 10^3 sperm ml^{-1} for bivalves (Styan and Butler, 2000).

Knowledge of hydrodynamic conditions that optimise reproduction in apex species, such as asteroids, is important for predicting their population ecology as well as for management of marine systems. Asteroids are known to be extremely important in the structuring of some marine ecosystems (Paine, 1969, 1980; Uthicke, 2009). At high population densities, some asteroid species can cause negative effects and

require management. An example of this is for *Acanthaster planci*, the crown-of-thorns sea star, where outbreaks can cause widespread reef-building coral mortality events and active culling measures are put in place to prevent damage to important reef systems (Bos et al., 2013). Asteroids can also cause negative impacts to commercial bivalve fisheries (Lawrence, 2013). Population densities are highly variable (Uthicke et al., 2009) and the prediction of harmful population outbreaks and efficacy of management approaches depends on knowledge of the environmental and biological controls on recruitment (Bos et al., 2013; Caballes and Pratchet, 2017).

The objective of this study was to examine whether individual sea stars could profitably use behavioural mechanisms to improve fertilisation success by modifying their local hydrodynamic regime. This study applied hydrodynamic theory and laboratory experiments to determine key constraints on reproduction in asteroids using both flat and arched postures in a range of flow fields.

2. EXPERIMENTAL METHODOLOGY

The experimental work was undertaken in a unidirectional flow channel measuring 7.50 m long and 0.30 m wide. Flow rate was controlled using a pump and two depth-averaged flow velocities (flow velocity averaged over the entire depth of the water column) were investigated. These were 0.10 ms^{-1} and 0.25 ms^{-1} and corresponded to relatively “low” and "high” turbulence cases. A sluice gate located downstream of the experimental section was used to control the water depth (Fig. 2), which was set at 0.15 m or 0.30 m during the experiment.

Both sandy (smooth) and rocky (rough) substrates were simulated in the flume. The rough surface consisted of dental plaster slabs into which 40 mm diameter spheres were irregularly set and subsequently removed (Dams, 2015). To simulate sand, skateboard grip tape with a mean particle diameter of 240 μm (equivalent to a fine to medium sand) was affixed to the flume base.

Life sized models were 3D printed in 21 separate components and assembled into flat and arched positions. To simulate the spiny aboral surface, the plastic models were coated in latex and submerged in coarse sand of variable grain size. The flat model measured 16 cm between the tips of opposing arms. The arms of *Asterias rubens* are broad at the base and taper gradually towards the tip (Hayward and Ryland, 1995). For this study, the arms of the model averaged ≅20 mm in width, which was consistent with the mean width derived from measurements of specimens of *A. rubens* collected from Plymouth Sound for this study. The identically proportioned arched model measured 60 mm from the substrate to the base of the central disc, with the mean distance from the oral to aboral side of the central disc measuring 17 mm. The models therefore represented typical specimens within recorded size limits (Hayward and Ryland, 1995). A pressure-sensitive adhesive was used to secure the models to the substrate.

The neutrally buoyant tracer dye Rhodamine was used to represent spawned male gametes. To recreate a natural spawning event, the dye would have needed to have been discharged at ten locations representing the gonopores, which open aborally on the interradial surface of each side of all five arms. Mimicking the exact release locations was not possible in this study and dye was released from a single point

151 source. As well as facilitating the laboratory experiments, a single point source is
152 consistent with the assumptions of the analytical model applied in this study to
153 interpret the laboratory results (equation 1, detailed in section 3, from Denny 1988).
154 A central oral (underside) location was chosen to provide a conservative estimate of
155 dispersal potential. A single-point aboral release on the upstream interradius would
156 be expected to overestimate dispersal compared with natural conditions, with
157 release points sheltered behind the arms and disc. Following an oral side release,
158 dye encircled the arms of the models within the flume, which has been observed in
159 the field in both *Asterias rubens* and *Martasterias glacialis* (Naylor, 2011). As a
160 result, all estimates of dye dispersal should be taken as minimum values. The dye
161 was injected at an initial concentration of $2x10^5$ ppb using a gravity-fed syringe.
162
163 Dye concentration was measured at four positions downstream of the model along
164 the flume centreline using a Turner Designs C3 Submersible Fluorometer sampled at
165 1 Hz. The base of the device was 6 cm from the substrate for the arched model and
166 1 cm from the substrate for the flat model. Data extracted from the Fluorometer was
167 used to quantify the decay of dye concentration with distance downstream of the
168 measurement section. The measured distances downstream of the model were 0.10
169 m, 0.20 m, 0.50 m and 1.00 m (Fig. 2).
170
171 Dye concentration data for both a flat and arched model were obtained for the
172 following flow conditions: (1) the “low” turbulence flow case with a depth-averaged
173 flow velocity, $\bar{u}$ = 0.10 ms^{-1} and Reynolds number, *Re* = 7500 (for a depth of 0.15 m
174 and assuming the flume to be an open channel regime with a free surface flow). (2)
175 the “high” turbulence flow case with $\bar{u}$ = 0.25 ms^{-1} and *Re* = 18750. Both flow

conditions were tested using the smooth, sandy substrate and the rough, rocky substrate. For each flow condition, the dye was released over a period of 100 seconds, which enabled stable measurements of dye concentration to be obtained.

A Nortek Vector Acoustic Doppler Velocimeter (ADV) was used to obtain direct point measurements of flow velocity through the flume cross-section, a distance 80 mm downstream of the model centre (Fig. 2). Measurements of all three velocity components (x – along-flume, y – cross-flume, z - vertical) were obtained for both depth-averaged flow velocities at 35 mm vertical intervals at three cross-flume measurement locations. Velocity data were recorded for a 15 second period at each instrument location and owing to the size of the instrument's measurement volume, no data could be obtained below 35 mm from the bed.

To analyse flow below this height, Digital Particle Image Velocimetry (DPIV) was used. This technique captured the details of the down-flume flow field local to the model in both the flat and arched positions. 30–80 μm hollow glass microspheres were chosen to be tracer particles owing to their neutral buoyancy and suitability for DPIV. The particles were imaged within a light sheet (1 m long, 5 mm wide) along the centre of the flume's primary (x) axis. The light sheet was created using a series of Cree X-RE white Light Emitting Diodes (LED) with collimated lenses, angled at 6°. The illuminated tracer particles were filmed using a Canon EOS 7D Mark II camera (50 frames per second; 1/200 shutter speed, F4, ISO 16000) in otherwise dark conditions. The 0.10 ms^{-1} "low" turbulence flow velocity was investigated using DPIV. Velocity vectors (u, w) throughout the camera field of view were computed from image sequences using the DPIV Matlab application, 'PIVLab' (Thielicke and

Stamhuis, 2014a, 2014b, Thielicke 2014). DPIV is a Lagrangian approach for measuring particle velocities within a fluid, observing from a stationary standpoint and tracking particle movement from frame to frame.

For the plan view visualisation, black food colouring was injected at a single point on the oral side of the model's central discs to simulate the release of gametes and the flow was filmed from above.

3. ANALYTICAL MODEL DESCRIPTION

This study applied an analytical model (Denny, 1988; Denny and Shibata, 1989) to laboratory-measured values in order to calculate downstream sperm concentration C for an external spawning event in a turbulent environment. It is assumed that the turbulent water column moves at a mean velocity $\bar{u}$ and sperm are released at a constant rate from a single point source at a distance x upstream from released ova. The model is based on a steady-state solution of the turbulent advection-diffusion equation:

$$C = \frac{Q_s \, \bar{u}}{2 \, \pi \, \alpha_y \, \alpha_z \, u_*^2 \, x^2} \quad (1)$$

where:

$\bar{u}$ = mean velocity in the *x*-direction.

u_* = shear velocity.

x = downstream distance.

Q_s = sperm release rate.

α_y and α_z are coefficients that relate shear velocity to horizontal and vertical diffusivity.

225 Shear velocity u_* is a parameter which enables shear stress to be represented in
226 units of velocity. Denny (1988) noted that in a turbulent flow, shear velocity values
227 exceeding 5% of the mean flow velocity can be considered significant.

228 $$u_* = \sqrt{\frac{\tau_R}{\rho}} \quad (2)$$

229 In equation (2), ρ is the fluid density and τ_R is the Reynolds stress:

230 $$\tau_R = \rho \bar{u}' \bar{w}' \quad (3)$$

231 where $\bar{u}'$ and $\bar{w}'$ are the mean fluctuating components of the horizontal and vertical
232 flow velocities respectively. As with previous studies involving other echinoderms
233 (Denny, 1988; Denny and Shibata, 1989; Young et al., 1992), it is the velocity
234 fluctuations of u' and w', owing to vertical mixing by waves in the nearshore
235 environment, and resulting shear velocities that will be considered in this study.
236 The sperm release rate Q_s is calculated using the following equation (Young et al.,
237 1992):

238 $$Q_s = \frac{(S\, V_m)}{T_s} \quad (4)$$

239 Where:

240 S is the sperm concentration / ml.

241 V_m is the gonad volume.

242 T_s is the time in seconds.

243

244 Baker and Tyler (2001) list the sperm concentrations S of various externally
245 spawning species; *Asterias rubens* produce a typical concentration of 2.5 x 10^5
246 sperm ml^{-1} (Williams, 1999). The duration of a spawning event T_s for moderately
247 proportioned specimens (< 30 cm diameter) of the North Atlantic sea star

Marthasterias glacialis is 2400 seconds (Minchin, 1987). To calculate V_m, ten *A. rubens* specimens were collected from the waters of Plymouth Sound in two stages, four in February 2015 and six in October 2015. The specimens varied in size from 9 - 18 cm in diameter, with a mean diameter of 13 cm, and were opened aborally. Gonad colour was assumed to be consistent with *Protoreaster nodosus*, therefore the specimens were all male, having cream/white gonads – as opposed to yellow or orange gonads found in females (Bos et al. 2008). The gonads were removed and the eviscerated bodies weighed and measured. Utilising gonad indices data (taken as three for October and six for February) from Barker and Nichols (1983), the approach of Pearse (1965) was used to estimate the gonad weight:

$$gonad\ weight = \frac{eviscerated\ wet\ weight\ x\ gonad\ index}{100} \quad (5)$$

The measurements were used to calculate specimen volume and subsequently find the specific organ weight and density in order to calculate the volume of a single gonad, using:

$$\rho = \frac{m}{v} = \frac{\gamma}{g} \quad (6)$$

Where:

γ is the specific organ weight.

m is the mass.

v is the volume.

g is gravity, taken as 9.81 ms^{-2}.

ρ is the density of the organ.

The volume of a single gonad was related linearly to the eviscerated wet weight of a specimen. The mean wet weight of 30 grams was used to obtain a mean gonad volume of 12 cm^3 (Fig. 3). This volume is within the typical range of a previous study

concerning *Pisaster ochraceus,* a sea star species comparable in size with *Asterias rubens* (Sanford et al., 2009) and indicates a sperm release rate, Q_s value = 1.25 x 10^3 sperm/second applying (eq. 4).

The coefficients of horizontal and vertical spread α_y and α_z were calculated based on the approach detailed by Denny (1988), Denny and Shibata (1989) and Young et al. (1992), in which

$$\alpha_y = 1.6\alpha_z \quad (7)$$

and: $$\alpha_z^2 = K_z / u_*^2\ t \quad (8)$$

where t is the time since release and K_z is the vertical diffusivity in cm^2s^{-1} which can be calculated as:

$$K_z = \kappa\ u_*\ s \quad (9)$$

where:

κ is von Karmans constant, 0.41

s is the height of sperm release, measured from the substratum to the base of the spawning specimen.

Using equation (1), the theoretical decay rate of downstream sperm concentration is exponential, resulting in a monomial equation:

$$y = ax^k \quad (10)$$

Where:

k is the slope of the straight line, or gradient. The slope descends from left to right and has a negative value of -1.0

a is the value on the y axis corresponding to $x = 1$.

y is downstream concentration

297 x is length downstream from the spawning specimen

298

299 ## 4. RESULTS

300 ### 4.1 Concentration gradients

301 Rhodamine concentrations measured downstream of the arched model – used as a
302 proxy for sperm concentration – were universally higher, by up to an order of
303 magnitude, than those for the flat posture (Fig. 4) and higher concentrations were
304 measured at the lower flow rate of 0.10 ms^{-1} over both substrates in comparison to
305 the higher flow rate of 0.25 ms^{-1}. The lower flow rate and rough substrate induced
306 the highest concentrations at a distance of ≤0.20 m (Fig. 4b). A sharp decline in
307 concentration from the initial level of 2 x 10^5 ppb was experienced within the first
308 0.20 m for both postures in all environments. While the flat model resulted in lower
309 concentrations at both 0.10 and 0.20 m, the rate of decay between 0.10 and 0.20 m
310 was most pronounced with the arched posture. In all four environments, the
311 concentration decays according to a power law with the best fit exponent for the
312 arched posture was consistently higher than the theoretical value of -1.00, while the
313 flat model decay rate was lower.

314

315 Application of equation (1) using Q_s = 1.25 x 10^3 sperm/second, an assumed mean
316 velocity $\bar{u}$ value of 0.25 ms^{-1}, and a shear velocity u_{*uw} value of 0.0125 ms^{-1} (5% of
317 $\bar{u}$), theoretically shows a decline of two orders of magnitude occurring within the first
318 0.10 m, followed by a further decline of one order of magnitude from 0.10 m to a
319 downstream distance of 1.00 m. The laboratory results (Fig. 4) are consistent with
320 this and the measurement taken 0.10 m downstream of the model was 10^3 ppb,
321 reduced from the initial release concentration of 10^5 ppb. Despite a sharp decline in

concentration from 0.10 to 0.20 m, the laboratory results also show decays of one order of magnitude from 0.10 to 1.00 m as there is a considerably lower rate of decay occurring between 0.20 and 1.00 m for both flow rates and surfaces.

4.2 Effect of posture on flow fields

Flow velocity data obtained from the ADV demonstrated greatly reduced flow velocities in the wake, directly downstream of the model for both the flat and arched models (Fig. 5). For the flat model, the lowest velocities occurred along the flume centreline at the lowest measured elevation (35 mm from the substrate). For the arched cases, the minimum flow velocity occurred directly downstream of the central disc of the sea star model at $z \cong 0.08$ m, with $\bar{u}$ increasing slightly below this level, ensuring the mean velocities are non-zero at the elevation of sperm release. Mean flow velocities in the cross-flume and vertical directions ($\bar{v}$ and $\bar{w}$) were close to zero in all cases. Mean, fluctuating velocity components were used to estimate shear velocities in the range 0.004 to 0.031 ms^{-1} through the flume cross-section and indicated that shear stresses were highest adjacent to the bed and directly downstream of the sea star body in both flat and arched positions.

The DPIV measurements highlight the differences in the nature of the wake for the flat and arched sea stars (Fig. 6). For the arched model, flow is possible both above and below the central disc of the sea star and the size of the downstream wake is relatively small. By contrast, flow is close to zero below the flat model and the model presents a larger projected surface area to the flow at the elevation of the central disc because the arms and disc are at the same elevation. This ensures that the wake downstream of the flat body is larger in extent and the velocity vectors show

evidence of negative mean flow velocities, indicating stronger recirculation than for the arched case where measured mean velocities are always positive in the x-direction. The extent of the wake downstream of the flat model is further enhanced on the rough surface where flow separation occurs over some of the roughness elements. Evidence from the flow visualisation experiment (Fig 7) indicates dye accumulation between the limbs of the flat model (corresponding to the downstream gonopore locations) and in the stronger wake, and this effect is enhanced by the concave bedforms on the rough bed.

4.3 Analytical model results

To examine the influence of mean and shear velocity on a theoretical spawning event, equation (1) was applied for the arched model in both the “low” and “high” turbulence test cases. Sperm release rate Q_s was taken as 1.25 x 10^3 sperm/second and s, the release height above the substrate, was taken as 6 cm. The highest theoretical downstream concentrations occurred with the “low” turbulence case (Fig. 8a), when shear velocity was lowest (0.008 ms^{-1}), resulting in a vertical diffusivity, K_z = 1.97 cm^2s^{-1}. The results for the rough and smooth bed cases were comparable, implying minimal influence from the substrate. The lowest theoretical downstream concentrations were estimated for the “high" turbulence case on the rough surface, where measured shear velocities were greatest (up to 0.03 ms^{-1}), resulting in a higher K_z value of 4.43 cm^2s^{-1}. This agrees with the measured concentration data presented in Fig. 4, where small differences were observed between rough and smooth substrates and the lowest dye concentrations were recorded for $\bar{u}$ = 0.25 ms^{-1} on the rough surface.

372 ## 5. DISCUSSION

373 ### 5.1 The influence of posture and environment

374 Hydrodynamic forces play a central role in the ecology of nearshore environments,
375 influencing individuals (including their survival, morphology, movement, feeding and
376 reproduction) as well as population and community dynamics in space and time
377 (Denny 2006). The flow environment is known to lead to behavioural responses (e.g.
378 in gastropods; Denny, and Blanchette, 2000) as well as other responses (such as
379 phenotypic plasticity in shell size and shape in gastropods; Trussell 1997). Most
380 organisms, including both sea star models investigated here, present a bluff body
381 (an immersed body where drag force created by the flow is dominated by pressure
382 drag) to oncoming flow, thus at sufficient Reynolds numbers flow separation occurs
383 leading to the formation of a low-pressure wake region of recirculating flow in the lee
384 of the organism (Koehl, 1977,1982), which may enhance mixing of gametes
385 (Crimaldi and Zimmer, 2014). Our flow visualisation results (Figs 6, 7) show that
386 when in the flat position, turbulent mixing in the mean flow is low and released dye
387 accumulates between pairs of limbs and in the relatively large downstream wake
388 region. As a result, the dye remains trapped close to the body of the sea star for
389 considerable periods (although probably not long enough for gametes to become
390 ineffective, which takes around$\leq$ 2 h for the sea star *Acanthaster planci*; Benzie and
391 Dixon, 1994) and is only slowly advected into the mean flow from a diffuse, rather
392 than point source.
393
394 Although turbulent mixing will ultimately dilute gamete concentrations excessively, at
395 intermediate levels the role of physical stirring by turbulent flow is thought to be the
396 primary process responsible for the successful meeting of gametes, at least at the

physical scales investigated here (> 1mm; Crimaldi and Zimmer, 2014). By expending energy in arching, the sea star minimises the trapping effect and enhances dispersion and mixing of gametes in the mean flow, leading to concentrations an order of magnitude larger than for the flat case at a distance of 0.10 m downstream of the model (Fig 4). Our estimates of downstream dye concentrations may be slightly too high, particularly in the arched case, as a result of the single point release used. In a natural spawning event, gametes would be released from ten gonoporial point sources, which would make the initial release more diffuse.

Our results show that turbulent mixing is increased in both higher flow and over rougher substrates. The roughness Reynolds number, an index of boundary layer turbulence (Denny and Shibata, 1989), is increased by shear velocity and bed roughness. The higher flow velocity over the rough surface assessed in this study resulted in shear velocities up to 0.03 ms^{-1} (in excess of 5% of mean flow, a level thought significant; Denny, 1988) as well as high Reynolds numbers which may be sufficient to limit effective reproduction. These results suggest that asteroids would benefit from intermediate flow environments for spawning on a rough seabed, which has been hypothesised elsewhere (e.g. McEuan, 1988) but appears not to have been rigorously tested in field conditions. As shown by our results, rough surfaces enhance the wake effect, increase the turbulence levels adjacent to the bed and lead to higher dispersion of gametes, particularly as mean flow velocity is increased. However, while a difference in the theoretical downstream concentrations for varying hydrodynamic conditions (Fig. 8a) is evident, it is considerably smaller than differences observed between the arched and flat models. Therefore, although the

environment plays a role in creating favourable spawning conditions, behavioural modifications by the sea star create the principal advantage.

Like asteroids, other echinoderms, including holothurians (McEuen, 1988) and crinoids (Hendler and Meyer, 1982), also make behavioural changes to elevate their gonopores during spawning. The crinoid *Capillaster multiradiatus* adopts a stationary, extended arm posture to minimise vertical diffusivity. Individual sea cucumbers have been observed to adopt a raised, more upright posture, thus lifting spawned gametes higher in the benthic boundary layer. Adverse hydrodynamic conditions appear to further motivate behavioural modification, with holothurians observed swaying their body and increasing tentacle motion possibly to create extra turbulent mixing to compensate for low flow conditions (McEuan 1988).

Although arching is important in reducing trapping of gametes behind the organism (as seen in section 4.1 and 4.2), it may not be favourable to increase the height above the substratum to the full capacity of the sea star. The results of the Denny (1988) model (section 4.3) indicate that a low release point within the benthic boundary layer is preferable in order to maximise downstream concentration from a point source by minimising turbulent vertical diffusivity K_z, which increases with distance from the bed (equation 9). A further consideration is that maximising downstream concentration by minimising K_z comes at the expense of a reduction in total mixing and thus reduces the area over which gametes are spread. Arching enables gametes to be released freely into the water column, but the height at which they are released represents a compromise between retaining sufficient downstream concentration to achieve fertilisation success (lower release point) while ensuring

some mixing to increase the area over which gametes are spread (higher release point). Therefore, it may be necessary for larger individuals to only partially arch their bodies to achieve this balance, and in some cases smaller sea stars may have a hydrodynamic advantage which could enhance their reproductive potential and partially offset the expected advantage of increased fecundity in individuals with larger body size (Ramirez Llodra, 2002). This effect could also be important in enhancing reproductive success in high density populations where body size may be reduced (Levitan, 1991). We have not been able to find experimental evaluations of partially arched sea stars, but observations (e.g. Himmelman et al., 2008) show large specimens of *Asterias vulgaris* clearly not arching to their full capable height alongside fully arched smaller specimens.

5.2 The requirement for aggregation

Our results highlight the potential for rapid dilution of gametes downstream of a spawning echinoderm. At a downstream distance of 0.10 m, the rate of dye concentration decay (Fig. 4) in our experiment is greater than that observed for the irregular echinoid *Clypeaster rosaceus* (Levitan and Young, 1995), where in lower flow rates of 0.06 – 0.14 m/s two orders of magnitude difference in concentration of fluorescein dye were recorded at ≅ 0.20 m. However, consistent with the Young et al., (1992) study using the echinoid *Stylocidaris lineata*, our results showed that a higher mean velocity $\bar{u}$ resulted in a lower downstream sperm concentration. The rapid rate of concentration decay for the arched position observed in this study between 0.10 and 0.20 m suggests the maximum advantage offered by the arched position is in very close proximity to the sea star. Our results highlight the challenges

of external reproduction (Denny and Shibata, 1989) and explain common observations of aggregation behaviours in externally reproducing taxa (Yund, 2000).

Considering the optimal downstream sperm concentration studies for gastropods (Baker and Tyler, 2001) and bivalves (Styan and Butler, 2000), it is reasoned that the downstream sperm concentration for Asteroidea should not fall below 10^2 sperm ml^{-1} for favourable reproductive conditions. Therefore, assuming the neutrally buoyant rhodamine dye injected at comparable concentrations to a natural gamete release represents a reasonable proxy for male gamete dispersal, the results indicate that males and females should aim to arch and congregate at a distance of ≤ 0.10 m during spawning to maximise chances of fertilisation success. In line with previous studies concerning the benefits of close aggregation during external reproduction (Denny and Shibata, 1989; Pennington, 1985), our results demonstrate little reproductive benefit to the sea star in congregating at distances ≥ 0.20 m, and highlight the importance of maintaining high population densities through aggregation, especially with small-to-intermediate sized populations (Levitan and Young, 1995).

In contrast, Babcock et al. (1992) suggest high density aggregation is not required for *Acanthaster planci* and successful fertilisation can take place at distances of tens of metres. Babcock et al. (1992) use a sperm release rate Q_s five orders of magnitude higher than the figure used for *Asterias rubens* in this study. Young et al., (1992) suggest close aggregation is not required for *Stylocidaris lineata,* with sperm concentrations high enough for 50+% successful fertilisation indicated at a distance downstream of 6 m. However, the initial sperm concentration S used for *Stylocidaris*

lineata is five orders of magnitude higher than that of *Asterias rubens*, resulting in Q_s being four orders of magnitude higher. Reducing Q_s by an order of magnitude can reduce the distances over which 50% effective fertilisation can take place by 2–3 m (Young et al., 1992). It is suggested that close aggregation is universally advantageous for successful external fertilisation, irrespective of variable Q_s.

Water depth influences hydrodynamic regimes, as reducing the cross-sectional area of the water column proportionately increases flow velocity. The sea star *Protoreaster nodosus* has been observed to congregate in shallow water during the reproductive season (Bos et al. 2008). With high density aggregation in shallow areas, populations maximise exposure to velocities capable of generating sufficient turbulence, particularly important on smoother, sandy substrates. Additionally, shallow waters typically experience greater ranges of temperature, a potential trigger factor for spawning (Hancock 1958; Mercier and Hamel, 2009). Minchin (1987) recorded aggregations of *Marthasterias glacialis* specimens, common from the sublittoral to depths of around 180 m (Villalobos et al. 2006), spawning in shallow water where temperature increase is maximised.

While the laboratory study reported here attempts to simulate certain aspects of marine conditions, a unidirectional flume cannot reproduce the fluctuations in flow velocity and direction to which a marine spawning event would be subjected (Gaylord, 2000). In a natural environment, with sperm and ova being subjected to variable flow directions (within a narrow range of angles), aggregating in high densities may be even more important**.** A further consideration is whether natural spawning is precisely synchronous at all. The analytical model (Denny, 1988)

assumes sperm shed from a source upstream moving directly downstream towards ova shed at a constant rate. Caballes and Pratchett (2017) discovered through laboratory experiments that male specimens of *Acanthaster planci*, are more susceptible to environmental cues such as temperature change and are first to spawn, with pheromones from the released sperm triggering females (and further males) to spawn. Close-proximity, high density aggregation would improve and hasten pheromone detection. This study suggests that any interval between male and female spawning in close congregation should be a matter of seconds rather than minutes. As noted above, released gametes may remain effective for up to 2 h (Benzie and Dixon, 1994) for sea stars, but they are at risk of diffusion from excessive turbulence and predation (Hendler and Meyer, 1982).

Enhanced knowledge of asteroid reproduction may be used to improve environmental management, or improve the ability to predict changes in sea star populations. For example, the ability to aggregate may be a key determinant of minimum viable population sizes which is valuable knowledge for managers who wish to either protect vulnerable species or limit the spread of undesirable species, such as *Acanthaster planci*. Optimal spawning locations may be predictable from topography, hydrodynamic modelling, or the distribution of prey species populations such as *Mytilus edulis* (Uthicke et al., 2009). Temporally and spatially limited spawning aggregations are vulnerable to anthropogenic disturbances and may be foci of effective management actions. The close density aggregation required for successful reproduction can have further negative consequences for sea stars when populations are subjected to predation by crustaceans or demersal fish (Ravelo et al., 2017) or affected by an outbreak of disease such as sea star wasting disease,

546 which has decimated populations local to the North American Pacific coast from Baja
547 California to Alaska (Menge et al., 2016). Mass mortality events impact upon the role
548 of the sea star in the top-down control mechanisms needed to maintain species
549 diversity in intertidal ecosystems (Paine, 1980). Such mortality events are expected
550 to increase with rising sea temperatures resulting from climate change (Bates et al.,
551 2009).
552

553 **5.3 Conclusions**

554 Sea stars increase the chance of successful fertilisation by adopting an arched
555 position. Hydrodynamic conditions also contribute to fertilisation success. The lower
556 flow case of 0.10 ms^{-1} over both rocky and sandy substrates generated favourable
557 levels of turbulence, with the rocky substrate proving most advantageous at a
558 distance $\leq$ 0.20 m. The reproductive benefits of adopting an arching posture are
559 greater than benefits derived from seeking favourable environmental conditions in
560 terms of flow, seabed roughness and resultant turbulence. Based upon this study, it
561 is predicted that in a natural spawning event, fertilisation success would increase in
562 high density aggregations, with distances between males and females ideally being
563 no greater than 0.10 m.
564

565 **ACKNOWLEDGEMENTS**

566 The authors would like to thank C Whittaker for help with the light box design.
567 Additional help was provided by R Nokes, D Wain, S Simoncelli, W Bazeley, N Price,
568 G Stewart, W Guy, E Walker, R Jackson, J Wong, J Cox, W Thielicke, E Stamhuis, P
569 Blondel, L Firth, A Harvey, P Rendle, W H P Thomas. We thank C Mah for useful
570 discussions leading to this research and P Naylor for figure 1b.

571 DJ was supported by UK Natural Environment Research Council National Capability
572 funding. All data supporting this paper are openly available from the University of
573 Bath data archive at https://doi.org/10.15125/BATH-00387.

574

575 **REFERENCES**

576 Babcock, R.C., Mundy, C.N. and Whitehead, D., 1994. Sperm diffusion models and
577 in situ confirmation of long-distance fertilization in the free-spawning asteroid
578 Acanthaster planci. *The Biological Bulletin*, *186*(1), pp.17-28.

579 Baker, M.C., Tyler, P.A., 2001. Fertilization success in the commercial gastropod
580 *Haliotis tuberculata*. Mar. Ecol. Prog. Ser. 211, 205–213.

581 Barker, M.F., Nichols, D., 1983. Reproduction, recruitment and juvenile ecology of
582 the starfish, *Asterias rubens* and *Marthasterias glacialis*. J. Mar. Biol. Assoc.
583 U.K. 63, 745–765.

584 Bates, A.E., Hilton, B.J., Harley, C.D., 2009. Effects of temperature, season and
585 locality on wasting disease in the keystone predatory sea star *Pisaster*
586 *ochraceus*. Dis. Aquat. Org., 86(3), pp.245-251.

587 Benzie, J.A.H. and Dixon, P., 1994. The effects of sperm concentration, sperm: egg
588 ratio, and gamete age on fertilization success in crown-of-thorns starfish
589 (*Acanthaster planci*) in the laboratory. Biol. Bull, 186(2), pp.139-152.

590 Bos, A.R., Gumanao, G.S., Alipoyo, J.C. and Cardona, L.T., 2008. Population
591 dynamics, reproduction and growth of the Indo-Pacific horned sea star,
592 *Protoreaster nodosus* (Echinodermata; Asteroidea). Mar. Biol. 156(1), pp.55-
593 63.

594 Bos, A.R., Gumanao G.S., Mueller, B., Saceda-Cardoza, M.M.E., 2013.
595 Management of crown-of-thorns sea star (*Acanthaster planci* L.) outbreaks:

596 Removal success depends on reef topography and timing within the
597 reproduction cycle. Ocean Coast Manage. 71:116-122.
598 Caballes, C.F., Pratchett, M.S., 2017. Environmental and biological cues for
599 spawning in the crown-of-thorns starfish. PloS one, 12(3), p.e0173964.
600 Clark, A.M., 1968. Starfishes and Their Relations. Natural History Museum
601 Publications, London.
602 Crimaldi, J.P., Zimmer, R.K., 2014. The Physics of Broadcast Spawning in Benthic
603 Invertebrates. Ann. Rev. Mar. Sci. 6 (1), 141-165.
604 Dams, B., 2015. An Investigation into Hydrodynamics and Arching Sea Stars.
605 University of Bath Dissertation.
606 Denny, M.W., 1988. Biology and the mechanics of the wave-swept environment.
607 ISBN 0-691-08487-4. Princeton Paperbacks.
608 Denny, M.W., Shibata, M.F., 1989. Consequences of surf-zone turbulence for
609 settlement and external fertilization. Amer. Naturalist 134, 859–889.
610 Denny, M.W., Blanchette, C.A., 2000. Hydrodynamics, shell shape, behavior and
611 survivorship in the owl limpet Lottia gigantea. J. Exp. Biol. 203 (17), 2623-
612 2639.
613 Denny, M.W., 2006. Ocean waves, nearshore ecology, and natural selection. Aquat.
614 Ecol. 40 (4), 439-461.
615 Gaylord, B., 2000. Biological implications of surf-zone flow complexity. Limnol.
616 Oceanogr. 45 (1), 174-188.
617 Hancock, D.A., 1958. Notes on starfish on an Essex oyster bed. J. Mar. Biol. Assoc.
618 U.K. 37, 565–589.
619 Hayward, P.J., Ryland, J.S., 1995. Handbook of the Marine Fauna of North West
620 Europe. Oxford University Press, Concise Edition.

621 Hendler, G. and Meyer, D.L., 1982. Ophiuroids flagrante delicto and notes on the
622 spawning behaviour of other echinoderms in their natural habitat. Bull. Mar.
623 Sci. 32(2), pp.600-607.
624 Hillewaert, H., 2000. *Asterias rubens* on the Belgian Continental Shelf. Studio Image.
625 Himmelman, J.H., Dumont, C.P., Gaymer, C.F., Vallières, C. and Drolet, D., 2008.
626 Spawning synchrony and aggregative behaviour of cold-water echinoderms
627 during multi-species mass spawnings. Mar. Ecol. Prog. Ser. 361, pp.161-
628 168.
629 Koehl, M.A.R., 1977. Effects of Sea Anemones on the Flow Forces They Encounter.
630 J. Exp. Biol. 69 (1), 87-105.
631 Koehl, M.A.R., 1982. The Interaction of Moving Water and Sessile Organisms. Sci.
632 Am. 247 (6), 124-134.
633 Lawrence, J., 2013. Starfish: Biology & Ecology of the Asteroidea. Johns Hopkins
634 University Press, Baltimore, MD, USA.
635 Levitan, D.R., 1991. Influence of Body Size and Population Density on Fertilization
636 Success and Reproductive Output in a Free-Spawning Invertebrate. Biol.
637 Bull. 181 (2), 261-268.
638 Levitan, D.R., Sewell, M.A., Chia, F.S., 1991. Kinetics of fertilization in the sea urchin
639 *Strongylocentrotus franciscanus*: Interaction of gamete dilution, age, and
640 contact time. Biol. Bull. 181(3), 371–378.
641 Levitan, D.R., Young, C.M., 1995. Reproductive success in large populations:
642 empirical measures and theoretical predictions of fertilization in the sea
643 biscuit *Clypeaster rosaceus*. J. Exp. Mar. Biol. Ecol. 190(2), pp.221-241.
644 McEuen, F.S., 1988. Spawning behaviors of northeast Pacific sea cucumbers
645 (Holothuroidea: Echinodermata). Mar. Biol, 98(4), pp.565-585.

646 Menge, B.A., Cerny-Chipman, E.B., Johnson, A., Sullivan, J., Gravem, S., Chan, F.,
647 2016. Sea Star Wasting Disease in the Keystone Predator *Pisaster*
648 *ochraceus* in Oregon: Insights into Differential Population Impacts,
649 Recovery, Predation Rate, and Temperature Effects from Long-Term
650 Research. PLoS One 11 (5), e0153994.
651 Mercier, A., Hamel, J.-F., 2009. Endogenous and Exogenous Control of
652 Gametogenesis and Spawning in Echinoderms. Adv. Mar. Biol. 55, 1-302
653 Minchin, D., 1987. Sea-water temperature and spawning behaviour in the seastar
654 *Marthasterias glacialis*. Mar. Biol. 95, 139–143.
655 Naylor, P., 2011. Great British Marine Animals. ISBN: 978-09522831-6-4. Sound
656 Diving Publications, Third Edition.
657 Nichols, D., Barker, M.F., 1984. A comparative study of reproductive and nutritional
658 periodicities in two populations of *Asterias rubens* (Echinodermata:
659 Asteroidea) from the English Channel. J. Mar. Biol. Assoc. U.K. 64, 471–
660 484.
661 Paine, R.T., 1969. A note on trophic complexity and community stability. Amer.
662 Naturalist 103(929), 91–93.
663 Paine, R.T., 1980. Food Webs: Linkage, Interaction Strength and Community
664 Infrastructure. J. Anim. Ecol. 49 (3), 667-685.
665 Pearse, J.S., 1965. Reproductive periodicities in several contrasting populations of
666 *Odontaster validus* Koehler, a common Antarctic asteroid. Antarct. Res. Ser.
667 5, 39–85.
668 Pennington, J.T., 1985. The ecology of fertilization of echinoid eggs: The
669 consequences of sperm dilution, adult aggregation and synchronous
670 spawning. Biol. Bull. 169, 417–430.

671 Ramirez Llodra, E., 2002. Fecundity and life-history strategies in marine
672 invertebrates. Adv. Mar. Biol.43, 87-170.
673 Ravelo, A.M., Konar, B., Bluhm, B., Iken, K., 2017. Growth and production of the
674 brittle stars *Ophiura sarsii* and *Ophiocten sericeum* (Echinodermata:
675 Ophiuroidea). Cont. Shelf Res., *139*, pp.9-20.
676 Sanford, E., Wood, M.E., Nielsen, K.J., 2009. A non-lethal method for estimation of
677 gonad and pyloric caecum indices in sea stars. Invertebr. Biol. 128, 372–
678 380.
679 Styan, C.A., Butler, A.J., 2000. Fitting fertilisation kinetics models for free-spawning
680 marine invertebrates. Mar. Biol. 137, 943–951.
681 Svendsen, I. A., 1987. Analysis of surf zone turbulence. J. Geophys. Res. 92:5115-
682 5124.
683 Thielicke, W., Stamhuis, E.J., 2014. PIVlab – Towards User-friendly, Affordable and
684 Accurate Digital Particle Image Velocimetry in MATLAB. J. Open Res.
685 Softw., 2: e30, DOI: http://dx.doi.org/10.5334/jors.bl (accessed 14.06.16).
686 Thielicke, W., Stamhuis, E.J., 2014. PIVlab - Time-Resolved Digital Particle Image
687 Velocimetry Tool for MATLAB (version: 7.10
688 R2010a). http://dx.doi.org/10.6084/m9.figshare.1092508 (accessed
689 14.06.16).
690 Thielicke, W., 2014. The flapping flight of birds - Analysis and application. PhD
691 dissertation, Rijksuniversiteit Groningen, Netherlands.
692 http://irs.ub.rug.nl/ppn/382783069 (accessed 13.06.16).
693 Trussell, G.C., 1997. Phenotypic plasticity in the foot size of an intertidal snail. Ecol.
694 78 (4), 1033-1048.

695 Vevers, H.G., 1949. The biology of *Asterias rubens* L.: Growth and reproduction. J.
696 Mar. Biol. Assoc. U.K. 28(1), 165–187.
697 Villalobos, F.B., Tyler, P.A., Young, C.M., 2006. Temperature and pressure tolerance
698 of embryos and larvae of the Atlantic seastars *Asterias rubens* and
699 *Marthasterias glacialis* (Echinodermata: Asteroidea): potential for deep-sea
700 invasion. Mar. Ecol. Prog. Ser. 314, 109-117.
701 Vogel H., Czihak G., Chang, P., Wolf, W., 1982. Fertilisation kinetics of sea urchin
702 eggs. Math. Biosci. 58, 189–216.
703 Williams, M.E., 1999. Fertilisation ecology of broadcast spawning marine
704 invertebrates. PhD dissertation, University of St. Andrews, Scotland, UK.
705 Williams, M.E., Bentley, M.G., 2002. Fertilization success in marine invertebrates:
706 The influence of gamete age. Biol. Bull. 202(1), 34–42.
707 Uthicke, S., Schaffelke, B., Byrne, M., 2009. A boom–bust phylum? Ecological and
708 evolutionary consequences of density variations in echinoderms. Ecol.
709 Monographs, 79(1), pp.3-24.
710 Young, C.M., Tyler, P.A., Cameron, J.L., Rumrill, S.G., 1992. Seasonal breeding
711 aggregations in low-density populations of the bathyal echinoid *Stylocidaris*
712 *lineata.* Mar. Biol. 113, 603–612.
713 Yund, P.O., 2000. How severe is sperm limitation in natural populations of marine
714 free-spawners? Trends Ecol. Evol. 15(1), 10–13.

715 **FIGURE CAPTIONS**

716 Figure 1: *Asterias rubens*, (a) flat (Hillewaert, 2000) and (b) arched (Naylor, 2011).

717

718 Figure 2: Schematic diagram of the flume and experimental apparatus.

719

720 Figure 3: Gonad volume as a function of eviscerated wet weight for ten *Asterias*
721 *rubens* specimens collected from Plymouth sound ($p<0.05$).

722

723 Figure 4: Dye concentration as a function of distance from the release point, x: a) $\bar{u}$,
724 mean velocity = 0.10 m/s, smooth surface (P = 0.05 arched, 0.10 flat) b) $\bar{u}$ = 0.10
725 m/s, rough surface (P = 0.12 arched, 0.07 flat) c) $\bar{u}$ = 0.25 m/s, smooth surface (P =
726 0.16 arched, 0.01 flat) d) $\bar{u}$ = 0.25 m/s, rough surface (P = 0.09 arched, 0.15 flat).
727 The dye concentration upon release at 0.00 m was 200,000 ppb, therefore all cases
728 experienced a large decline in concentration between 0.00 and 0.10 m, with the
729 greater decline experienced in all cases with the model in the flat position. Dotted
730 lines represent monomial equation trend lines. Note log 10 axes.

731

732 Figure 5: Contour plots of down-flume flow velocity data, measured using the ADV,
733 80 mm downstream in the *x*-axis of the sea star model with the upstream position of
734 the model superimposed. (a-b) $\bar{u}$, mean velocity = 0.1 m/s, smooth surface; (c-d) $\bar{u}$ =
735 0.1 m/s, rough surface; (e-f) $\bar{u}$ = 0.25 m/s, smooth surface; (g-h) $\bar{u}$ = 0.25 m/s, rough
736 surface. Note that no measurements were obtained in the range z = 0 m to z = 0.03
737 m owing to the limitations of the instrument.

738

739 Figure 6: Flow velocity vectors obtained from DPIV: (a) flat position and (b) arched
740 position. Vector directions indicate the flow direction at each point with the mean
741 flow from left to right. Velocity magnitude is linearly proportional to the vector length
742 where the vector length for the maximum local velocity of 0.1 m/s is provided.
743
744 Figure 7: Visualisation in plan view of dye release for (a) the arched model and (b)
745 the flat model, with flow from left to right.
746
747 Figure 8: Modelled sperm concentration C as a function of downstream distance x,
748 computed using Eq (1) based on measured hydrodynamic parameters for the arched
749 model.
750 a) Results for the range of responses observed in this study. Sperm release rate Q_s =
751 1.25 x 10^3 sperm/second. Values of mean velocity $\bar{u}$ and shear velocity $u_{*_{uw}}$ were
752 taken from Acoustic Doppler Velocimeter measurements.
753 b) Results for two heights from the substrate, s = 1 cm and s = 6 cm, simulating a flat
754 and arched model respectively. Sperm release rate Q_s = 1.25 x 10^3 sperm/second,
755 mean velocity $\bar{u}$ = 0.25 ms^{-1} and shear velocity $u_{*_{uw}}$ = 0.0125 m/s (5% of $\bar{u}$).
756

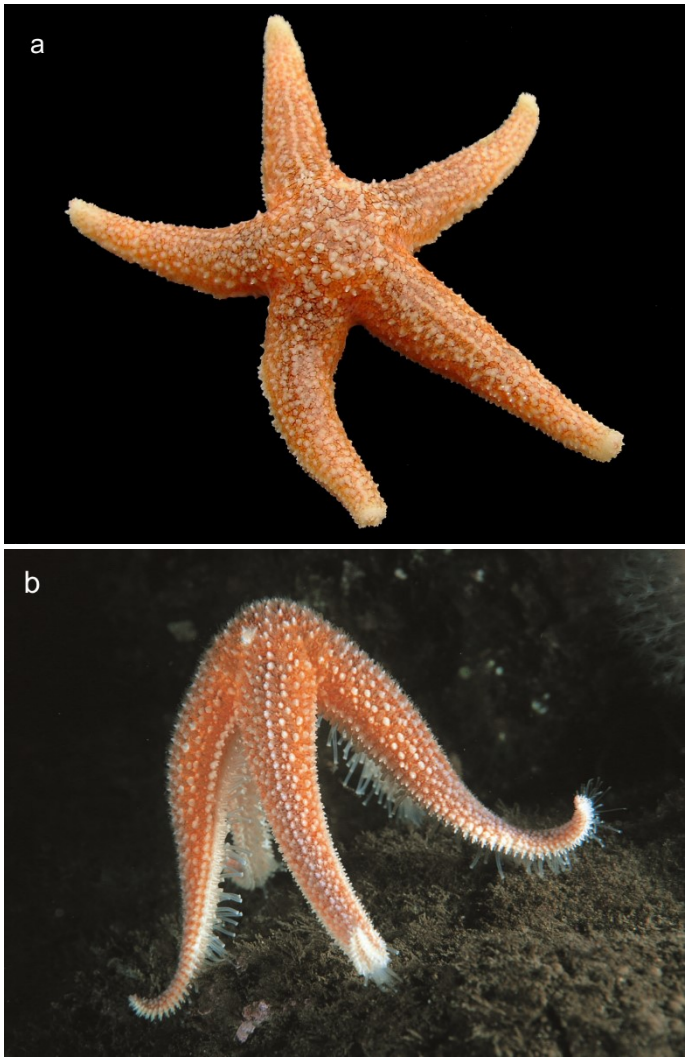
a
b

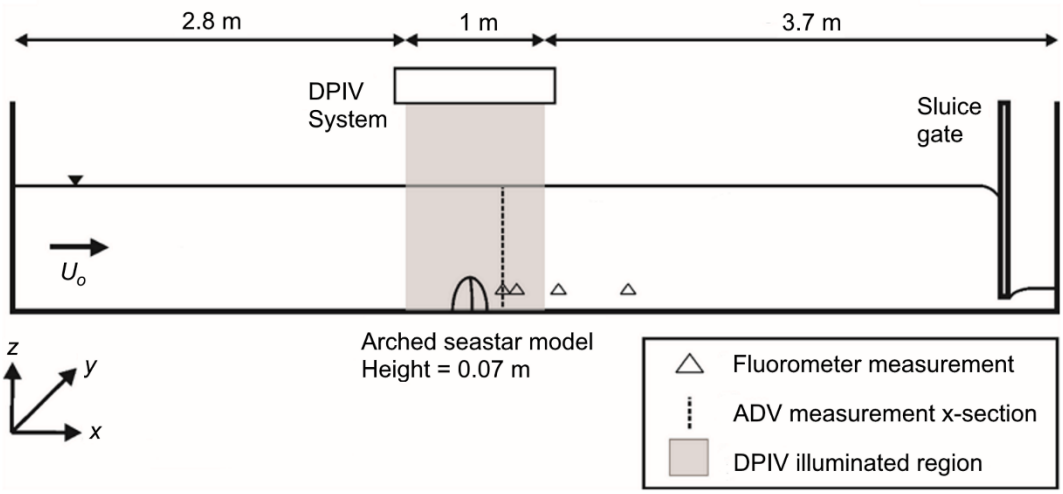

764

765

766

767

768

769

770

771

772

773

774

775

776

777

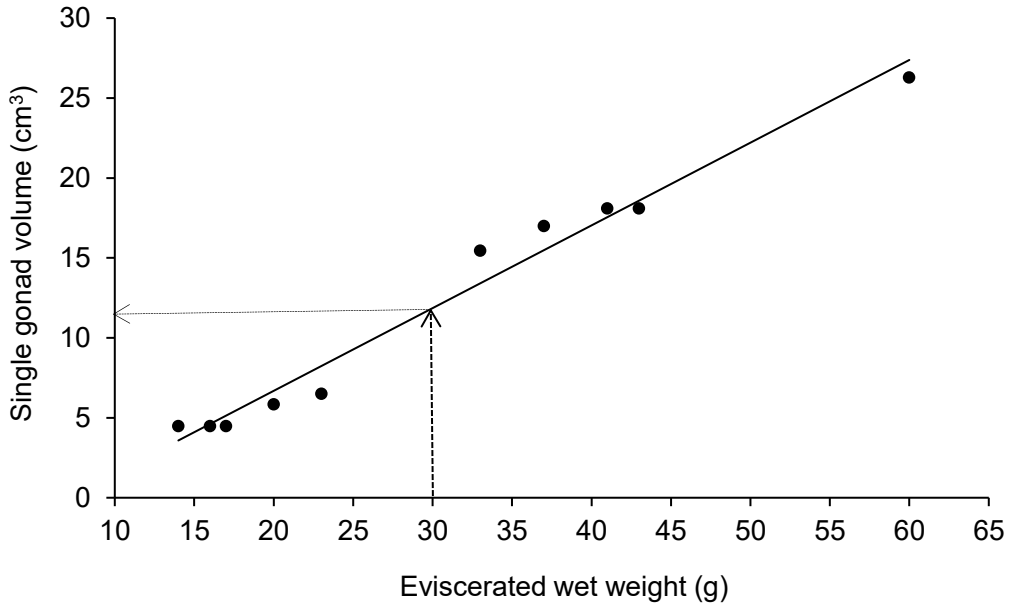

778

779

780

781

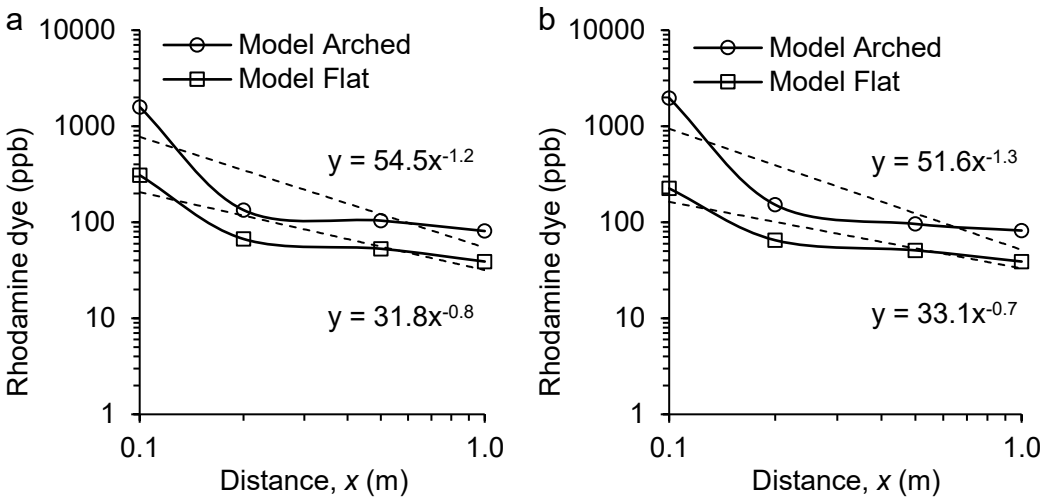
a
10000
1000
100
10
1
Rhodamine dye (ppb)
Model Arched
Model Flat
y = 54.5x-1.2
y = 31.8x-0.8
0.1
1.0
Distance, x (m)
b
10000
1000
100
10
1
Rhodamine dye (ppb)
Model Arched
Model Flat
y = 51.6x-1.3
y = 33.1x-0.7
0.1
1.0
Distance, x (m)

782

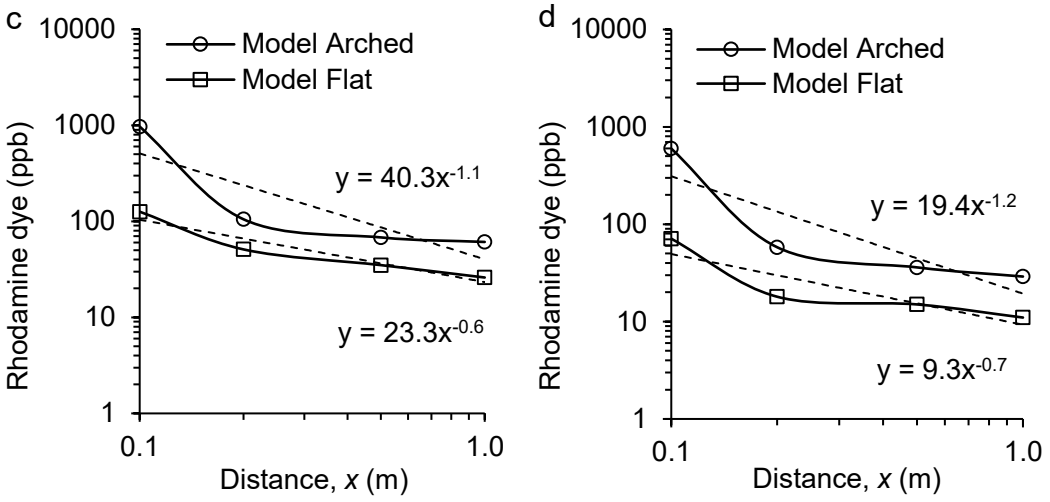
c
10000
1000
100
10
1
Rhodamine dye (ppb)
Model Arched
Model Flat
y = 40.3x-1.1
y = 23.3x-0.6
0.1
1.0
Distance, x (m)
d
10000
1000
100
10
1
Rhodamine dye (ppb)
Model Arched
Model Flat
y = 19.4x-1.2
y = 9.3x-0.7
0.1
1.0
Distance, x (m)

783

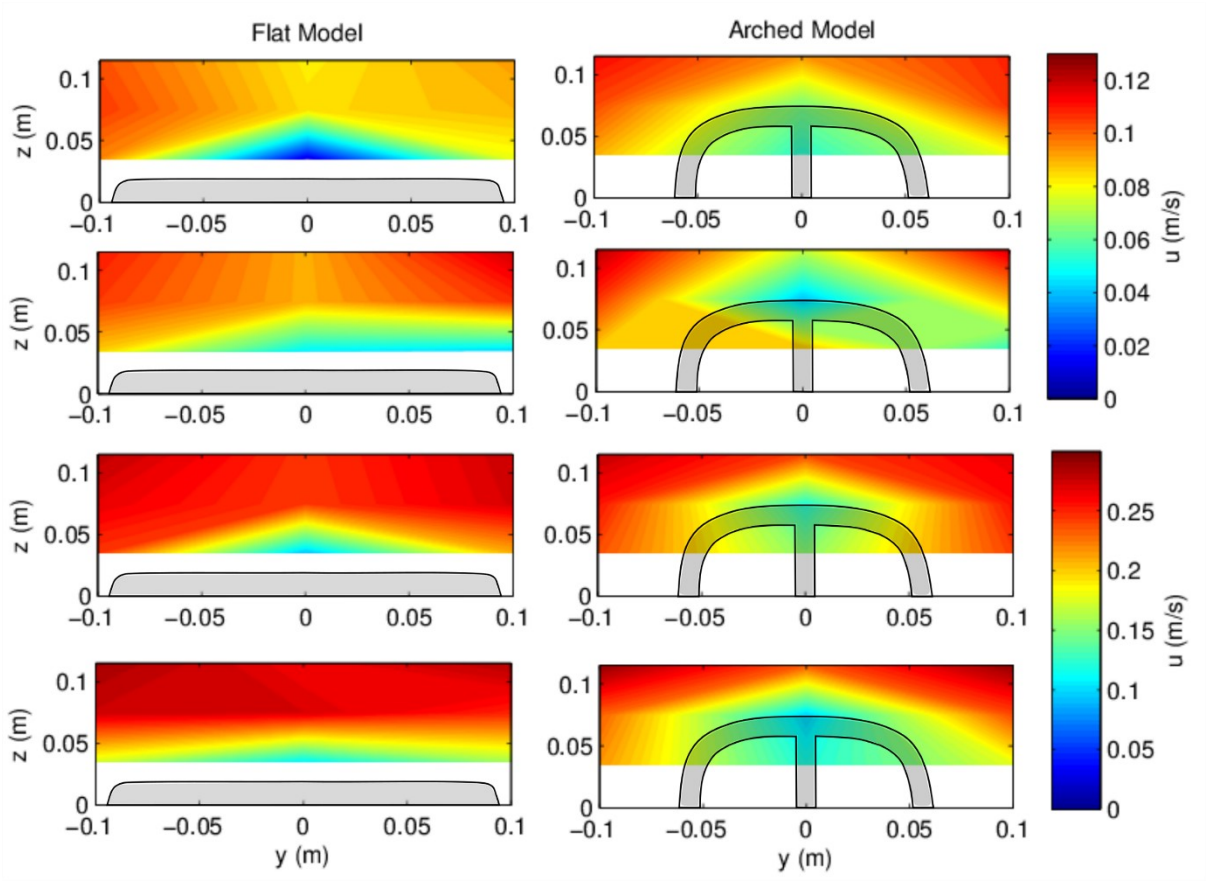
Flat Model
Arched Model
z (m)
y (m)
u (m/s)
0.1
0.05
0
−0.1
−0.05
0.05
0.12
0.08
0.06
0.04
0.02
0.25
0.2
0.15

784

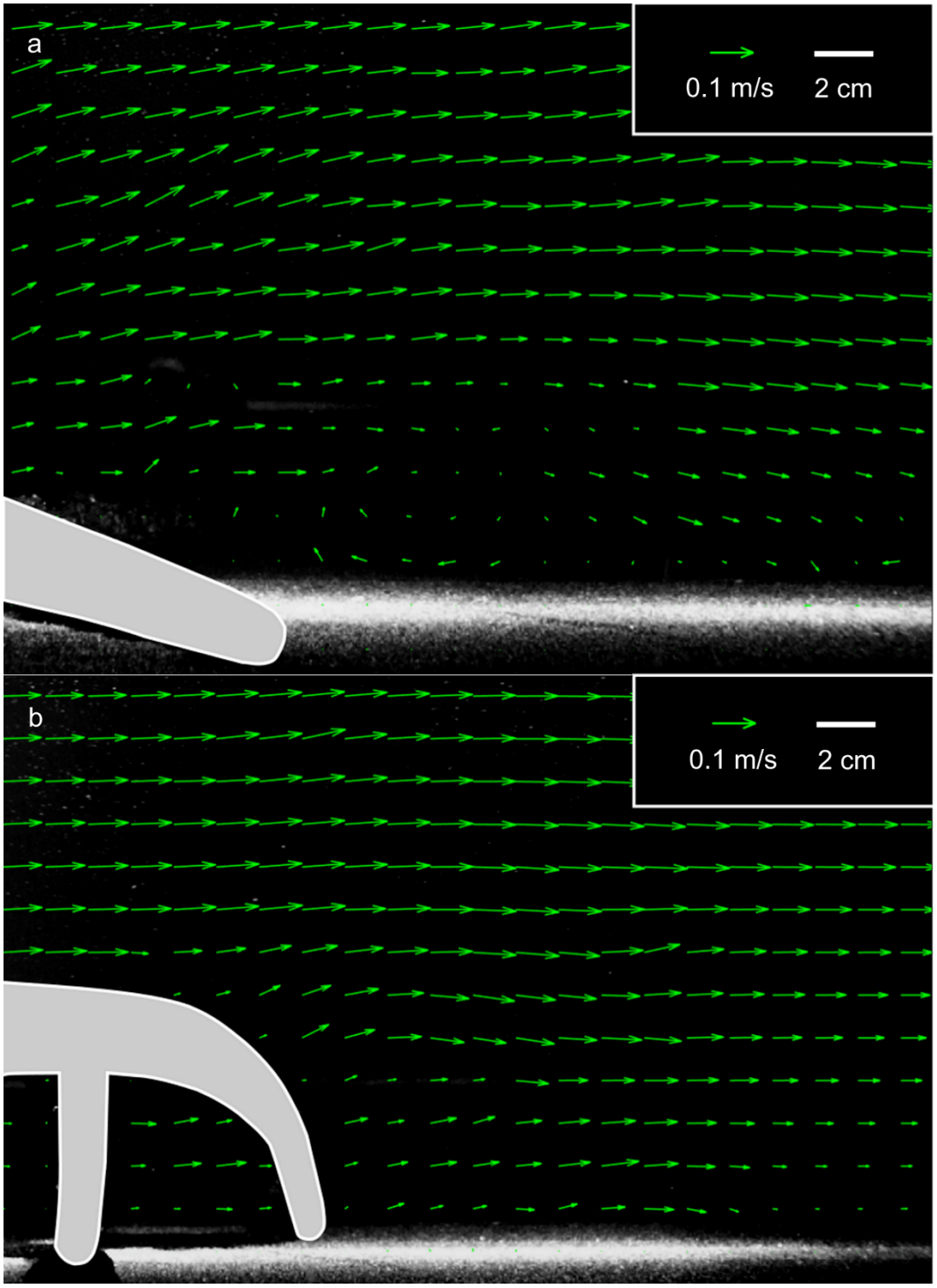

785

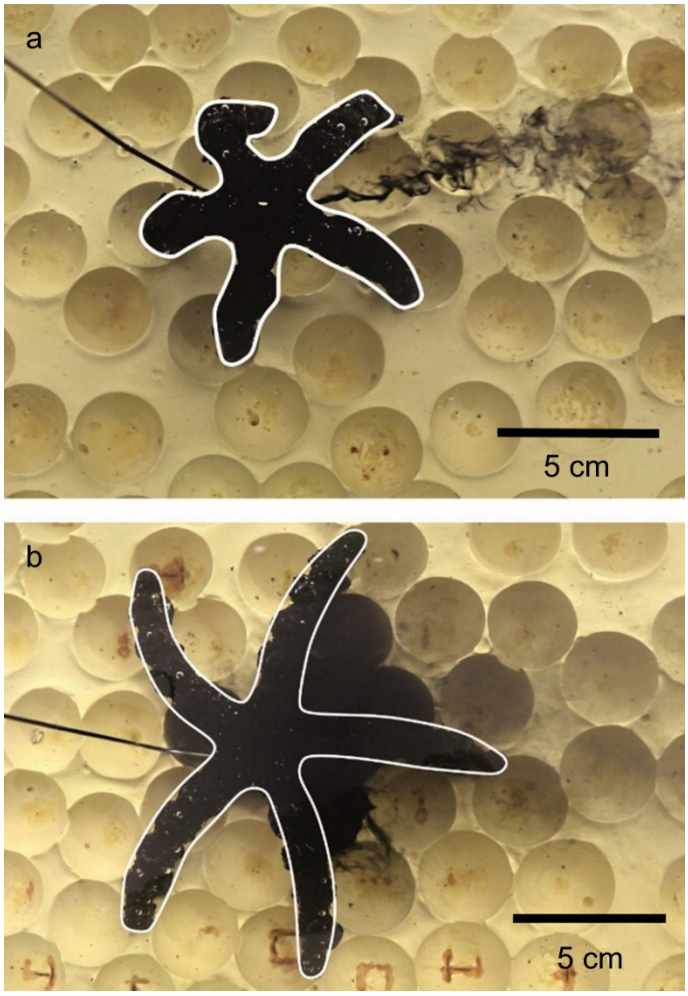

786

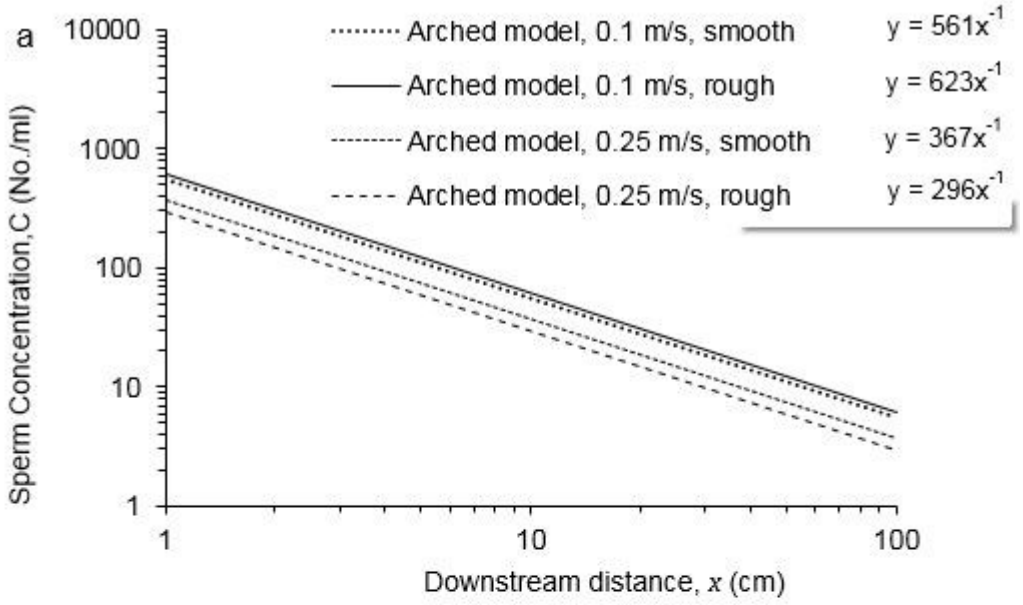
a
Arched model, 0.1 m/s, smooth
y = 561x-1
Arched model, 0.1 m/s, rough
y = 623x-1
Arched model, 0.25 m/s, smooth
y = 367x-1
Arched model, 0.25 m/s, rough
y = 296x-1
Sperm Concentration,C (No./ml)
10000
1000
100
10
1
1
10
100
Downstream distance, x (cm)

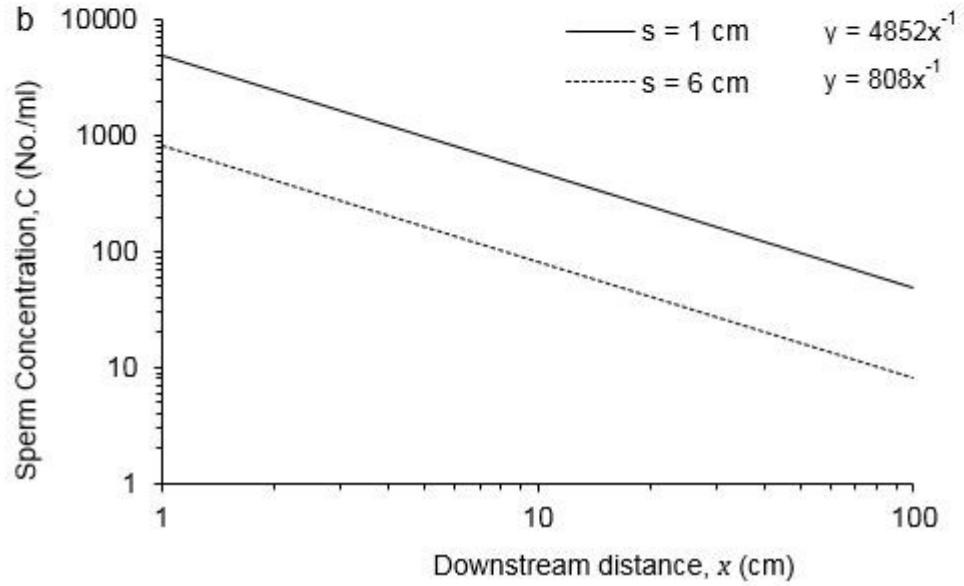
b
s = 1 cm
y = 4852x-1
s = 6 cm
y = 808x-1
Sperm Concentration,C (No./ml)
10000
1000
100
10
1
1
10
100
Downstream distance, x (cm)

787

788